BMC Gastroenterology

RESEARCH

Open Access

Comprehensive analysis of ferroptosis-related long non-coding RNA and its association with tumor progression and ferroptosis in gastric cancer

Shenglan Huang[1†], Kan Liu[1†], Queling Liu[1], Si Tao[1] and Hua Wang[1*]

Abstract

Gastric cancer (GC) is one of the most common malignant tumors with a poor prognosis. Ferroptosis is an distinct type of non-apoptotic cell death that is closely associated with tumor prognosis. Thus, we aimed to develop an novel prognosis risk model based on ferroptosis-related lncRNAs and excavate novel diagnostic markers. In this study, eight ferroptosis-related lncRNAs were obtained for constructing the prognosis model in GC based on TCGA database. The patients in the high-risk group had worse survival than those in the low-risk group, and the risk-grouping could be used as an independent prognostic factor for OS. Receiver operating characteristic curve analysis demonstrated this risk model was superior to traditional clinicopathological features in predicting GC prognosis. GSEA revealed that these lncRNAs were mainly involved in cell adhesion, cancer pathways, and immune function regulation. The key gene HAGLR of this risk signature was up-regulated in GC tissues and cells. Function assays showed that knockdown of HAGLR could effectively inhibit the GC cells proliferation and migration, whereas silencing HAGLR accelerated apoptosis and ferroptosis cell death process. In conclusion, we established a novel ferroptosis-related prognostic risk signature including eight lncRNAs, which may improve prognostic predictive accuracy for patients with GC.

Keywords Gastric cancer, Ferroptosis-related LncRNA, Prognostic model, HAGLR

Introduction

Gastric cancer (GC) ranks fifth in terms of cancer incidence rates and is the fourth leading cause of cancer-related mortality worldwide [1]. Although systemic chemotherapy, surgery, radiotherapy, targeted therapy, and immunotherapy have proven efficacy against GC, the prognosis of GC remains poor. According to statistics, the annual fatality rate of GC is approximately 10%, and the 5-year survival rate is less than 30% [2]. Currently, tumor size, lymph node metastasis, distant metastasis, stage, and pathological type of cancer are the main factors for prognosis [3]. However, the high heterogeneity in patients with GC may restrict the applicability of

†Shenglan Huang and Kan Liu contributed equally to this work and share first authorship.

*Correspondence:
Hua Wang
dcwanghua@126.com
[1]Department of Oncology, The Second Affiliated Hospital, Jiangxi Medical College, Nanchang University, No. 1, Minde Road, Nanchang, Jiangxi Province 330006, P.R. China

current prediction methods. Therefore, it is imperative to explore highly sensitive and specific molecular markers to improve the predictive accuracy and specificity of GC.

Ferroptosis, a novel and distinct type of nonapoptotic cell death, is characterized by the accumulation of iron-dependent reactive oxygen species (ROS), oxidization of polyunsaturated fatty acids (PUFAs), accumulation of lipid peroxides, and phospholipid peroxidation damage of cell membranes [4, 5]. Ferroptosis is closely associated with numerous biological processes, such as lipid metabolism, amino acid metabolism, iron metabolism, and glutathione metabolism [6]. In GC, ferroptosis has been found to be closely related to tumorigenesis, tumor microenvironment, and drug resistance, and may be used as a new oncological marker and potential therapeutic target [7, 8]. Recently, large-scale clinical trans-omics studies have contributed to the construction of reliable prognostic biomarkers based on ferroptosis-related genes in GC [9–12]. Nonetheless, mRNA signatures may provide imperfect predictions because of low tissue specificity and instability [13]. Hence, it is vital to discover novel ferroptosis-related biomarkers for GC prognosis.

Long noncoding RNAs (lncRNAs), which account for 80–90% of all ncRNAs and are structurally more than 200 nucleotides (nt) in length, have attracted widespread attention as cancer biomarkers for early disease diagnosis and prognosis [14]. LncRNAs have been reported to be associated with multiple biological functions, such as tumorigenesis and immune responses [15]. Notably, numerous studies claim that lncRNAs play a crucial role in regulating ferroptosis in cancer. LncRNAs can act as competitive endogenous RNAs to prevent oxidation, thereby inhibiting ferroptosis. Ferroptosis-related lncRNAs were also chosen as excellent indicators for predicting prognosis in multiple cancers, such as hepatocellular carcinoma [16], colon cancer [17], and head and neck squamous cell carcinoma [18]. However, the potential value of ferroptosis-related lncRNAs as prognostic indicators and therapeutic targets has not been fully explored in GC.

In this study, we aimed to construct a ferroptosis-related lncRNA prognostic model based on The Cancer Genome Atlas (TCGA) data and then explored the biological functions of ferroptosis-related lncRNAs in GC. A flowchart of this study is shown in Fig. 1A-B.

Materials and methods

Data acquisition and processing

High-throughput sequencing datasets of GC tissues, including 375 tumor samples and 32 normal control samples, were downloaded from The Cancer Genome Atlas (TCGA) database (https://portal.gdc.cancer.gov/). After removing the low expressed genes with an average value < 0.5, we obtained 930 lncRNAs and 12,952 protein-coding genes. After excluding GC patients with less than 30 days of follow-up time, the remaining 334 patients with completed survival information were assigned as the primary cohort, and half of these samples were randomly selected and assigned to the validation cohort ($N = 167$). Meanwhile, 259 ferroptosis-related genes were obtained from the FerrDb V1. database(http://www.zhounan.org/ferrdb/operations/download.html), which including 108 Driver, 69 Suppressor, and 111 Marker [19]. Some genes are included in more than one annotation group, with

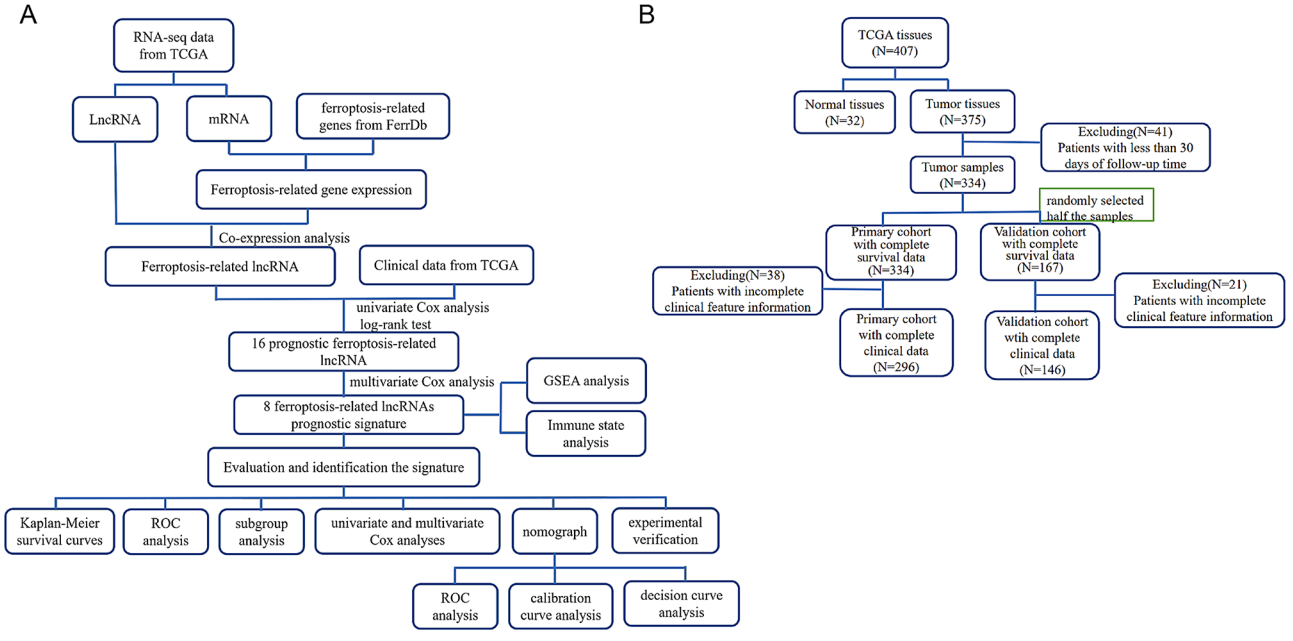

Fig. 1 Flowchart of the analysis. (**A**) The process of study conduction; (**B**) The screening process

14 genes found in both drivers and markers, 3 genes in both drivers and suppressors, 10 genes in both suppressors and markers, and 1 gene present in all groups. After removing the 28 multi-annotated genes, the remaining 259 ferroptosis-related genes was used for subsequent analysis.

Screening ferroptosis-related LncRNA in GC

In GC, a total of 217 ferroptosis-related gene matrices were extracted by using the "limma" package of R 4.0.4 software (http://www.r-project.org/). Pearson correlation analysis was performed to identify ferroptosis-related lncRNAs according to the criteria of|correlation coefficient| > 0.3 and $p < 0.001$. In total, 741 ferroptosis-related lncRNAs were screened for further verification.

Establishment and identification of a ferroptosis-related LncRNA prognostic model for GC

To extract the prognostic ferroptosis-related lncRNAs, we performed Univariate Cox regression analysis and Kaplan-Meier analysis. Next, we incorporated prognostic ferroptosis-related lncRNAs candidates into a multivariate Cox regression analysis to screen independent prognostic lncRNAs. Next, we established an optimum prognostic risk model based on the lowest Akaike information criterion (AIC = 1213) by using the "Survival" R package. The Kaplan-Meier analysis was used to evaluate the correlation between the prognostic ferroptosis-related lncRNAs and overall survival (OS). Subsequently, according to the multivariate Cox regression coefficient and expression value of lncRNAs, the risk score of each patient was evaluated using the risk score equation as follows:

risk score = coef (lncRNA1) × exp (lncRNA1) + coef (lncRNA2) × exp (lncRNA2) +…+ coef (lncRNAn) × exp (lncRNAn).

where coef (lncRNA) represents the regression coefficient and exp (lncRNA) is the expression value. The median risk score was used to divide GC patients into high- and low-risk groups. The Kaplan-Meier analysis was performed to assess the survival between the low- and high-risk groups. Meanwhile, stratification analysis was performed based on the following clinicopathological features: age (≤ 65 and > 65 years), sex (male and female), grade (grade 1–2 and grade 3), and clinical stage (stage I-II and stage III-IV); $p < 0.05$ was considered statistically significant. A time-dependent receiver operating characteristic (ROC) curve was constructed to evaluate the predictive accuracy of the prognostic model for 1-, 2-, and 3-year OS via the "survivalROC" R package.

Subsequently, Cox regression analyses were performed to explore whether the risk score model could be used as an independent factor for OS by integrating other clinicopathological factors, including age, sex, grade, clinical stage, and TNM stage. The prognostic results are presented as the HR and 95% CI, and a p value < 0.05 was considered to indicate statistical significance. A multi-indicator ROC (multi-ROC) curve was calculated to assess the predictive accuracy of the risk model for OS, and the area under the curve (AUC) of the ROC curve was calculated to estimate the sensitivity and specificity.

The relevance between prognostic ferroptosis-related lncRNAs and their coexpressed mRNAs was analyzed using the "ggalluvial" R package of Cytoscape 3.8.2 software (http://www.cytoscape.org/).

Construction and validation of the nomogram

Based on the risk score and clinical factors (including age, sex, grade, and clinical stage), we established a nomogram to predict the 1- and 3-year survival probability of patients with GC. We then performed internal verification to assess the predictive precision of this nomogram. A calibration curve was drawn to appraise the uniformity of the predicted results. A multi-ROC curve was used to assess the predictive accuracy of the nomogram model. Decision curve analysis (DCA) was used to estimate the net benefit of this nomogram, in which the abscissa represented the threshold probability and ordinates represented the net income.

Enrichment analysis

First, gene set enrichment analysis (GSEA; version 4.1.0) was performed to identify the differential pathways between the high- and low-risk groups and further analyzed the potential biological mechanisms of the ferroptosis-related lncRNA prognostic signature. The c2.cp.kegg.v7.4.symbols.gmt downloaded from the Molecular Signatures Database (http://www.gsea-msigdb.org/gsea/msigdb/collections.jsp) was used to identify the significantly enriched pathways based on the false discovery rate (FDR q-value) < 0.05. Afterward, differential expressed genes (DEGs) were screened between high- and low-risk groups with screening criteria of FDR < 0.05 and|log2FC|≥1. According to these DEGs, Gene Ontology (GO) analysis was conducted to explore the potential biological function of risk signature.

Immune cell infiltration and immune-related pathways

According to the ferroptosis-related lncRNA prognostic model, single-sample GSEA (ssGSEA) was conducted to quantitatively analyze the difference in the infiltration level of immune cells and immune-related pathways between the high- and low-risk groups by using the "gsva" and "GSEABase" R packages. The result was visualized using the "ggpubr" R package of boxplot. Statistical significance was set at $p < 0.05$.

GC tissues collection and ethics approval

A total of 27 paired GC tissues and adjacent non-cancerous tissues were collected from patients with GC who underwent tumor surgical resection at the Second Affiliated Hospital of Nanchang University from October 2024 and March 2025. This study was approved by The Second Affiliated Hospital of Nanchang University Medical Research Ethics Committee and met the Helsinki Declaration. Tissue samples were stored at – 80 °C before RNA extraction.

Cell lines and cell transfection

Human GC cell lines (SNU-1, NCI-N87, AGS, HGC-27) and the gastric epithelial cell line GES-1 were purchased from Procell (Wuhan, China). The cells were all propagated in Dulbecco's modified Eagle medium (DMEM; solaibio, Beijing, China) supplemented with 10% fetal bovine serum (Gibco, Grand Island, NY, USA), 100 μg/mL streptomycin and 100 U/mL penicillin at 37 °C in a 5% CO2 incubator.

To identify the biological role of HAGLR in GC cells, three short hairpin RNAs targeting HAGLR (shHAGLR-1, shHAGLR-2, shHAGLR-3) were designed by Hanheng Biotechnology (Shanghai, China). Targeted sequences for shHAGLR are as follows: shHAGLR-1 5'-TATTCAAACACACACCCACAC-3', shHAGLR-2 5'-CACACACCCACACACATCCTC-3', shHAGLR-3 5'-TGTAT TCTCTCCTCTCTCTCG-3', negative control (shCtrl) 5'-TTCTCCGAACGTGTCACGT-3'. shHAGLR plasmids and shCtrl were transfected into AGS and HGC-27 cells, respectively, and the transfection was performed by Lipo3000 transfection reagent (Invitrogen) according to the manufacturer's instructions. After 48 h of transfection, RT-qPCR was conducted to analyze the knockdown efficiency.

Reverse transcriptionquantitative PCR (RTqPCR)

Total RNA extracted from GC cells and tissues was isolated with TRIzol reagent (Invitrogen, Carlsbad, CA, USA) and reverse transcribed into complementary DNA (cDNA) using EasyScript One-Step gDNA Removal and cDNA Synthesis SuperMix (TransGen Biotech, Beijing, China). The genes expression was determined by TB Green Premix ExTaq II (TaKaRa, Dalian, China). The relative gene expression was calculated using the 2-ΔΔCq method with GAPDH as an endogenous control. The primers sequences are listed in Supplementary Table S1.

Western blot analysis and antibodies

The total protein from the GC cells was isolated via RIPA lysis buffer (Beyotime, Shanghai, China) and separated via 10% SDS–PAGE. The protein samples were transferred onto a PVDF membrane (Millipore, Schwalbach, Germany). The membrane was blocked in 5% defatted milk for 1 h and then incubated with the following primary antibodies at 4 °C overnight: anti-ACSL4 (1:4000, 22401-1-AP; proteintech, China), anti-GPX4 (1:5000, 30388-1-AP; proteintech, China), β-actin (1:5000, ab32572; Abcam, UK). The membranes were washed three times in TBST for 5 min and then incubated with secondary antibody for 1 h at 37 °C. Finally, the protein bands were incubated with an enhanced chemiluminescence (ECL) reaction reagent (US Everbright, Inc., Suzhou, China) and imaged with a gel image processing system.

Cell proliferation assays

Cell proliferation was analyzed by CCK-8 and colony formation assays. For the CCK-8 assay, a total of 2×10^3 transfected AGS and HGC-27 cells were seeded uniformly in 96-well plates. 10μL of CCK8 reagent was added to the cells at different time points (24, 48, 72, and 96 h after seeding), followed by incubation in the dark for 2 h at 37 °C. The absorbance was detected at 450 nm using an enzyme immune-assay analyzer (Bio-Rad, Hercules, CA, USA). For the colony formation assays, a total of 5×10^2 transfected AGS and HGC-27 cells were evenly seeded in each well of six-well plates and maintained at 37 °C in a 5% CO2 incubator for 14 days. Then, the cell colonies were fixed with 4% paraformaldehyde for 20 min and stained with 0.25% crystal violet for 10 min at room temperature. Colonies were counted and photographed by microscopy.

Flow cytometry

The role of HAGLR in GC cell apoptosis was determined using a FITC-Annexin V/PI apoptosis detection kit (F6012, US Everbright Inc., China) according to the manufacturer's instructions. The GC cells were collected after 48 h of transfection, washed three times with PBS, and resuspended in 100 μL of binding buffer. The cell suspension was stained with 5 μL of V-FITC and 5 μL of PI solution and incubated for 15 min in the dark. Then, another 400 μL of binding buffer was added to the cell suspension. Cell apoptosis was analyzed using a flow cytometer (FACSCalibur flow cytometer; BD Biosciences) and analysis software (BD CellQuest™ Pro Software version 1.2 (BD Biosciences).

Cell migration assay

Scratch wound-healing and transwell assays were used to detect cell migration ability. For the scratch wound-healing assay, a total of 5×10^5 transfected AGS and HGC-27 cells were uniformly seeded in 6-well dishes and grown to 90% confluency. Confluent cells were scratched with a sterile 200 μL pipette tip, washed three times with PBS, and cultured in DMEM without FBS. The cell images were acquired with an optical microscope system at 0

and 24 h. The cell migration rate was calculated with the following formula: Cell migration rate (%) = (1-scratch diameter/original scratch diameter) × 100%.

Transwell chambers with 8 μm pore size (TCS013024, JET BIOFIL, Guangzhou, China) were used to perform the transwell assay. The transfected AGS and HGC-27 cells (2 × 104) were cultured in the upper chamber with 200 μL serum-free medium, and the lower chamber was filled with 600 μL DMEM with 20% FBS. After 48 h of penetration, the lower chamber cells were fixed with 4% formaldehyde and stained in crystal violet solution for 15 min. Then, the number of migrated cells was photographed and counted under an inverted microscope at ×200 magnification.

ROS measurements

Dihydroethidium (DHE) staining was used to detecte intracellular reactive oxygen species (ROS) levels. The transfected AGS and HGC-27 cells were incubated with 5 μM DHE (Beyotime, China) at 37 °C for 30 min. After the incubation, wash the cells 3 times with PBS to remove unbound DHE. The nucleus were then stained with DAPI for 30 min. Finnally, The cells were observed with a fluorescent microscope following PBS washing.

MDA, GSH and Fe^{2+} assays

The transfected AGS and HGC-27 cells was lysed with ultrasonic cell lyser. The protein concentration in the supernatant was detected by use BCA protein colorimetric assay kit (Elabscience, China, E-BC-K318-M). The concentration of Fe^{2+}, GSH, and MDA in GC cells were detected using Fe^{2+} colorimetric assay kit (Elabscience, China, E-BC-K773-M), malondialdehyde (MDA) colorimetric assay kit (Elabscience, China, E-BC-K028-M), and glutathione(GSH) colorimetric assay kit (Elabscience, China, E-BC-K030-M), according to the manufacturers respective instructions.

Mitochondrial transmission electron microscopy observation

The transfected AGS and HGC-27 cells were fixed with 2.5% glutaraldehyde fixative solution at room temperature for 4 h, followed by 2% osmic acid fixative for 1.5 h. After dehydration in a gradient of ethanol, the samples were embeded in a 1:2 mixture of acetone and resin. Then, Ultrathin Sect. (70 nm) were cut, mounted on a copper mesh, and stained twice with 2% uranium acetate and lead citrate. Lastly, images were acquired using a transmission electron microscope.

Statistical analysis

Statistical analyses were performed using R software (https://www.r-project.org/, version 4.0.4) and SPSS ver sion 24 (IBM, New York, USA). The chi-square test was used to analyze the baseline characteristics of patients with GC. Cox regression analysis was used to build a prognostic model. The Renyi weighted test was used to evaluate the survival difference between the two risk groups. All experiments were repeated at least in triplicate. The data were analyzed via GraphPad Prism 9.0 (San Diego, CA, USA) and are represented as the mean ± standard deviation (SD). The Kolmogorov–Smirnov test was used for normality analysis, and unpaired Student's t test or one-way analysis of variance (ANOVA) (followed by Turkey's Honest Significant Difference test) was applied in multiple group comparisons of normally distributed variables. A p value<0.05 was considered to be statistically significant.

Results

Identification of ferroptosis-related LncRNAs in GC

First, the mRNA and lncRNA expression matrix and clinical information of 375 GC samples were acquired from the TCGA database. According to the exclusion criteria, the data of 334 patients with complete follow-up information and 296 patients with complete clinicopathological data were included in subsequent analysis (Fig. 1B). The clinical pathological features of patients with GC included in this study are shown in Table 1. Then, the data of 259 ferroptosis-related genes were downloaded from FerrDb V1. (Supplementary Table S2). The included information of 217 ferroptosis-related genes in GC was obtained from the TCGA database (Supplementary Table S2). According to the Pearson correlation coefficient analysis, 741 ferroptosis-related lncRNAs were identified.

Screening of prognostic ferroptosis-related LncRNAs in GC

Univariate Cox regression analysis (followed by Wald test) and Kaplan-Meier analysis (followed by Renyi test) were used to analyze the association between the expression of ferroptosis-related lncRNAs and the OS of GC patients. Among the 741 ferroptosis-related lncRNAs, 16 were identified as prognosis-associated lncRNAs that were significantly correlated with the survival of patients with GC, and the results are shown in Supplementary Table S3. Subsequently, eight lncRNAs were further filtered to construct a prognostic signature using multivariate Cox regression analysis based on the minimum AIC value (AIC = 1213), which were AL365181.3, MIR3142HG, PVT1, LINC01315, AL353804.1, HAGLR, AC005586.1, and AC245041.1. Among them, AL365181.3, MIR3142HG, PVT1, LINC01315, AL353804.1, and AC005586.1 were prognostic lncRNAs with HR < 1, and HAGLR and AC245041.1 were prognostic at-risk lncRNAs with HR > 1, as shown in Supplementary Figure S1. The Kaplan-Meier analysis showed that the expression of ferroptosis-related lncRNAs was significantly correlated with survival ($p < 0.05$), of

Table 1 Clinical pathological parameters of patients with gastric cancer basing on TCGA database

Characteristic	primary cohort ($n=296$)	validation cohort ($n=146$)	*p* value
Age(year)			0.734
<=65	135	69	
>65	161	77	
Gender			0.348
Male	186	85	
Female	110	61	
Tumor grade			0.452
G1	7	1	
G2	101	52	
G3	188	93	
Clinical stage			0.853
I	38	15	
II	97	49	
III	130	68	
IV	31	14	
T classification			0.9
T1	13	7	
T2	61	26	
T3	145	72	
T4	77	41	
N classification			0.826
N0	90	40	
N1	80	43	
N2	64	29	
N3	62	34	
M classification			0.918
M0	277	137	
M1	19	9	

Note: T, tumor size; N, lymph node; M, distant metastasis;

which AL365181.3, MIR3142HG, PVT1, LINC01315, AL353804.1, and AC005586.1 were positively correlated with survival, whereas the other two lncRNAs (HAGLR, AC245041.1) were negatively correlated with survival (Fig. 2A-H). Subsequently, we constructed a coexpression network of the eight ferroptosis-related lncRNAs and mRNAs using Cytoscape and Sankey diagrams. This network visually displayed the correlation among ferroptosis-related genes, ferroptosis-related lncRNAs, and risk types of lncRNAs (Supplementary Figure S2).

Construction and verification of a ferroptosis-related LncRNA prognosis model for GC

According to the eight ferroptosis-related lncRNAs and corresponding regression coefficients, the risk score of each patient was obtained according to the following formula:

risk score = (0.143 × HAGLR expression)+ (-0.212 × AC005586.1 expression)+ (-0.055 × AL365181.3 expression) + (-0.242 × MIR3142HG expression) + (-0.089 ×PVT1 expression) + (-0.192 × LINC01315 expression) + (-0.409 × AL353804.1 expression) + (0.025 × AC245041.1 expression).

A ferroptosis-related lncRNA prognostic signature was established, and patients with GC were divided into two groups: low- and high-risk groups (median value = 1.1064). Kaplan–Meier survival curves for OS demonstrated that patients in the high-risk group had poorer survival than those in the low-risk group ($p=1.81e-07$), as shown in Fig. 3A. Time-ROC curve analysis was performed to evaluate the precision of the prognostic model, and the results proved that the risk

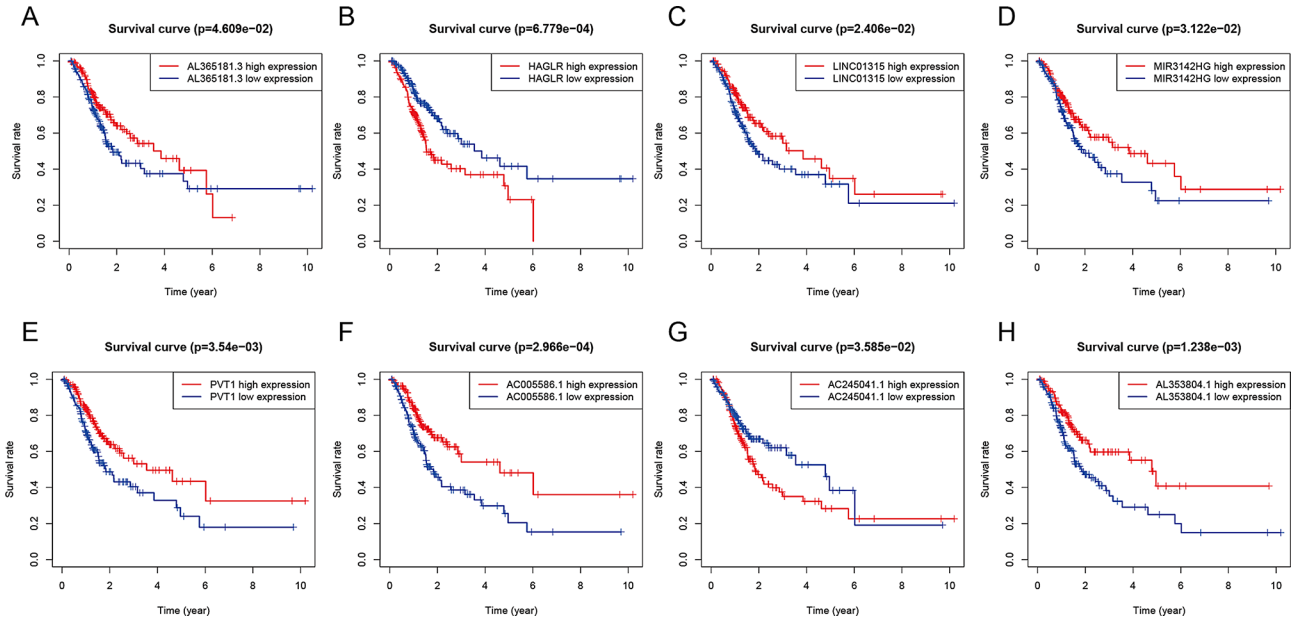

Fig. 2 The association between the eight ferroptosis-related lncRNAs and overall survival of patients with gastric cancer (**A**-**H**)

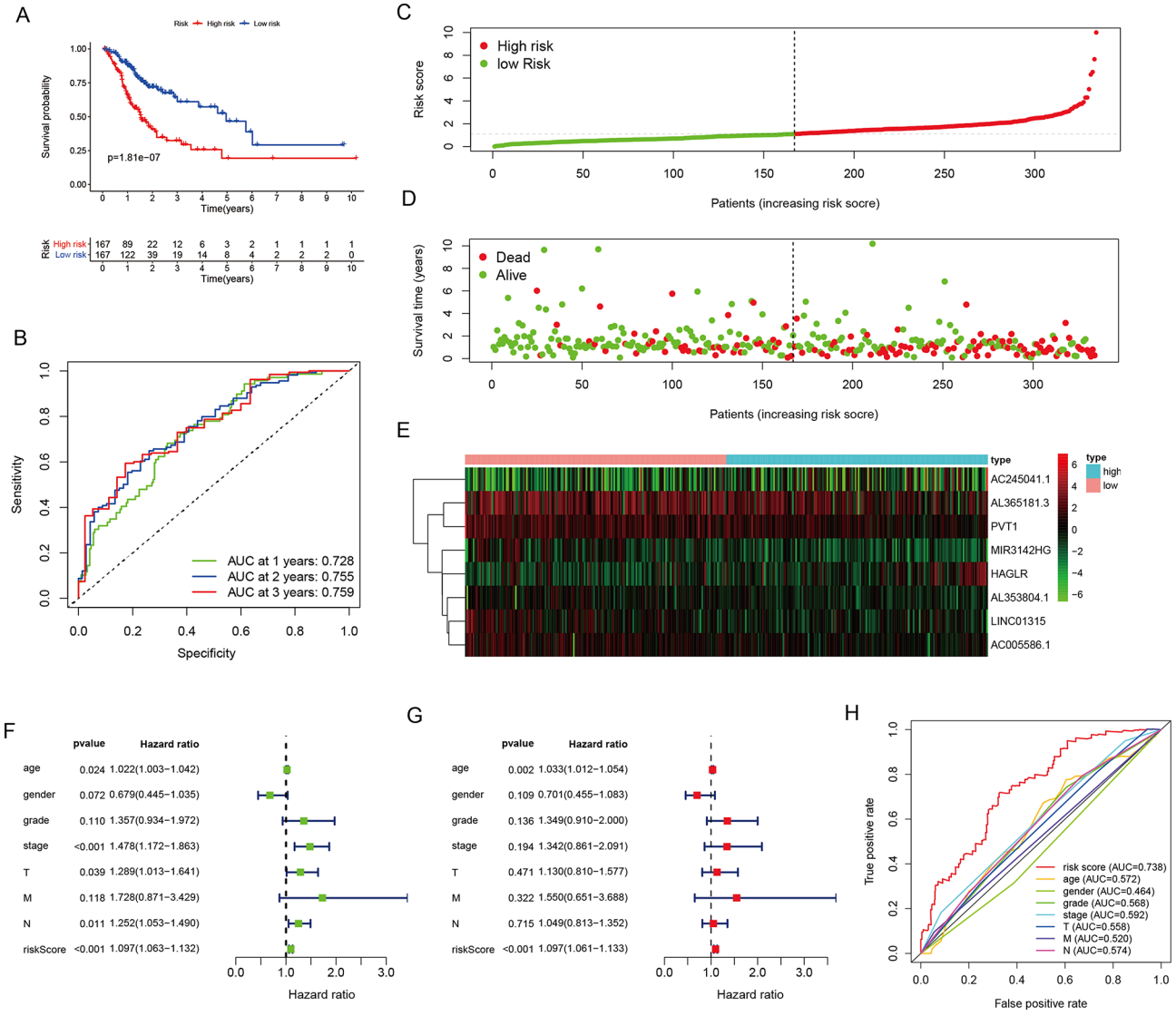

Fig. 3 Prognosis analysis of the eight ferroptosis-related lncRNAs signature in The Cancer Genome Atlas (TCGA) primary cohort. (**A**) Kaplan–Meier survival analysis of the high- and low-risk groups; (**B**) Time-dependent receiver operating characteristic (time-ROC) curve evaluated the precision of this prognostic model in 1-, 2-, and 3-year OS; **C**. The risk score curves based on the risk score of each patient; **D**. The scatter plots based on the survival status of each patient; the green dots represent living and red dots represent dead patients; **E**. The heatmap displayed the expression levels of the eight ferroptosis-related lncRNAs in the high- and low-risk groups; **F**. Univariate Cox regression analysis; **G**. Multivariate Cox regression analysis; **H**. Multi-indicator receiver operating characteristic (muti-ROC) curve analysis

model provided a precise predictive role, with AUC values for 1-, 2-, and 3-year OS of 0.728, 0.755, and 0.759, respectively (Fig. 3B). Risk score curves and scatter plots were drawn to explain the relationship between the risk score and survival status in patients with GC, and the results revealed that the higher the risk score was, the higher the mortality rate (Fig. 3C-D). The heatmap suggested that six lncRNAs (AL365181.3, MIR3142HG, PVT1, LINC01315, AL353804.1, and AC005586.1) were upregulated in the low-risk group, whereas the other two lncRNAs (AC245041.1 and HAGLR) were upregulated in the high-risk group (Fig. 3E). Furthermore, Univariate Cox analysis showed that age (HR = 1.022 (1.003 – 1.042), 95% CI: 1.003 – 1.042, $p = 0.024$), clinical stage (HR = 1.478, 95% CI: 1.172 – 1.863, $p<0.001$), tumor stage (T, HR = 1.289, 95% CI: 1.013 – 1.641, $p = 0.039$), node stage (N, HR = 1.252 (1.053 – 1.490), 95% CI: 1.053 – 1.590, $p = 0.011$), and risk score (HR = 1.097, 95% CI: 1.063 – 1.132, $p<0.001$) were associated with OS (Fig. 3F). Multivariate Cox regression analysis demonstrated that age (HR = 1.033, 95% CI: 1.012 – 1.054, $p = 0.02$) and risk score (HR = 1.097, 95% CI: 1.061 – 1.133, $p < 0.001$) were independent prognostic factors for patients with GC (Fig. 3G). Multi-ROC curves proved that the risk model provided a more precise predictive

role for survival than other clinical parameters (age, sex, grade, stage, T, N, M), with AUC = 0.738 (Fig. 3H).

In addition, we carried out verification analysis of the prognostic signature in the validation cohort and found that the survival probability in the high-risk group was significantly lower than that in the low-risk group ($p = 2.58e-06$), and the predictive validity of the AUC values for 1-, 2-, and 3-year survival was 0.760, 0.740, and 0.732, respectively(Fig. 4A-B). The results of the risk score curves, scatter plots, and heatmap in the validation group showed similar trends to those observed in the primary dataset (Fig. 4C-E). Cox regression and multi-ROC curves were performed in the validation group, as shown in Fig. 4F-H. The results indicated that the risk score was independently associated with survival in the validation group and that the risk score model was an excellent predictive indicator of prognosis compared with other clinical parameters with AUC = 0.771. The above results demonstrated that the ferroptosis-related lncRNA prognostic model had an accurate predictive ability for prognosis in patients with GC.

Subsequently, we adopted stratification analysis to estimate the relevance of risk scores and clinicopathological parameters. The results showed that patients in different

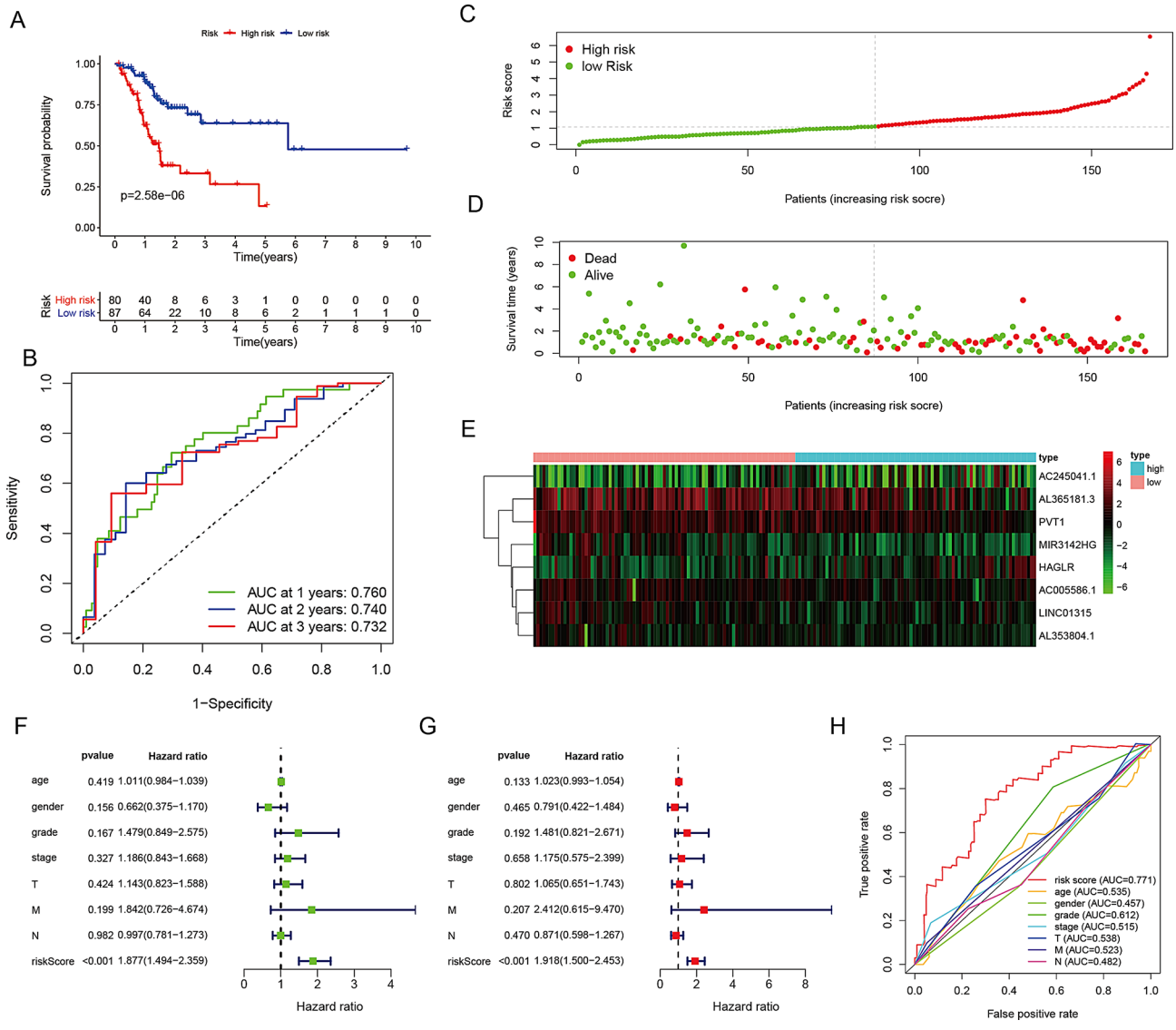

Fig. 4 Prognosis analysis of the eight ferroptosis-related lncRNAs signature in validation cohort. (**A**) Kaplan–Meier survival analysis of the high- and low-risk groups; (**B**) Time-dependent receiver operating characteristic (time-ROC) curve evaluated the precision of this prognostic model in 1-, 2-, and 3-year OS; **C**. The risk score curves based on the risk score of each patient; **D**. The scatter plots based on the survival status of each patient; the green dots represent living and red dots represent dead patients; **E**. The heatmap displayed the expression levels of the eight ferroptosis-related lncRNAs in the high- and low-risk groups; **F**. Univariate Cox regression analysis; **G**. Multivariate Cox regression analysis; **H**. Multi-indicator receiver operating characteristic (muti-ROC) curve analysis

subgroups had worse survival in the high-risk group, including age (≤ 65 and > 65 years), sex (male and female), grade (grade 1–2 and grade 3), and clinical stage (stage I-II and stage III-IV). This indicated that the prognostic signature was applicable to different subgroups (Supplementary Figure S3).

Construction and evaluation of the prognostic nomogram

A nomogram was established to predict the 1- and 3-year survival probability of patients with GC. The comprehensive score was calculated by combining each factor of age, sex, grade, clinical stage, and risk score. The results showed that the higher the total score was, the worse the prognosis (Fig. 5A). The accuracy and consistency of the nomogram were assessed using a calibration curve, multi-ROC curve, and DCA. The results of the calibration curve showed that the prognostic nomogram model was nearly in accordance with reality, as shown in Fig. 5B-C. Multi-ROC curve analysis demonstrated that the nomogram provided an accurate prediction ability with AUC = 0.769 for 1-year OS and 0.776 for 3-year OS (Fig. 5D-E), which was higher than the AUC value of the risk score and other clinical factors. The results of DCA demonstrated that the nomogram exhibited superior clinical practicality to traditional clinical parameters (tumor grade and clinical stage) in predicting the prognosis of patients with GC (Fig. 5F).

Function analysis of the ferroptosis-related LncRNA prognostic signature

GSEA was conducted to evaluate the potential biological mechanism of the ferroptosis-related lncRNA prognostic signature. According to the GSEA results, the high-risk group was positively related to 24 gene sets (P value < 0.05 and FDR < 0.25) and was closely related to "cell adhesion molecules", "cytokine and cytokine receptor interaction", "ECM receptor interaction", "Focal adhesion", "GAP junction", "TGF-β signaling pathway", "regulation of actin cytoskeleton", and "Hippo signaling pathway". Whereas low-risk group was enriched in "oxidative phosphorylation", "P53_signaling pathway", and "arachidonic acid metabolism", as shown in Supplementary Figure S4A. These pathways are mainly related tumor progression, ferroptosis and immune response. To further elucidate the biological functions of which risk signature might influence, we screened out DEGs between high- and low-risk groups. Then the DEGs was used for GO enrichment analysis, and the results of biological process (BP) showed that these DEGs were mainly enriched in "epithelial cell proliferation", "protein – lipid complex remodeling" and "lipoprotein particle remodeling" (Supplementary Figure S4B), which indicated that the risk signature may involve in cell proliferation and lipid metabolism in GC.

Immune cell infiltration and Immune-related pathways

Finally, ssGSEA was performed to discuss the immune state between the high- and low-risk groups by calculating the scores of 16 immune cells and 13 immune function-related pathways in patients with GC. The results revealed that the infiltration levels of immune cells, including B cells, DCs, iDCs, macrophages, mast cells, neutrophils, NK cells, pDCs, and Treg cells, were significantly upregulated in the high-risk groups ($P < 0.05$) (Supplementary Figure S4C). Regarding the immune-related pathways, APC costimulation, CCR, and type II IFN response were significantly upregulated in the high-risk group ($P < 0.05$) (Supplementary Figure S4D).

LncRNA expression levels in GC tissues and cells

To verify the expression levels of the eight ferroptosis-related lncRNAs, qRT – PCR was performed in 27 paird GC tissues. The results demostrated that the expression of AL365181.3, MIR3142HG, PVT1, LINC01315, AL353804.1, and AC005586.1 was decreased in GC tissues compared with adjacent normal tissues, whereas HAGLR and AC245041.1 was highly expressed in cancer tissues (Fig. 6A-H). It is seen that HAGLR was the most significantly up-regulated gene in GC tissues. The differential expression of HAGLR was verified in GC samples of TCGA datasets. The results also showed that HAGLR was highly expressed in GC specimens (Fig. 6I). We further investigated the relationship between HAGLR expression and clinicopathologic features. As shown in Fig. 6J-N, the results showed that patients with high Tumor(T) and Node(N) stages, and with distant metastasis tended to higher expression of HAGLR. Whereas, there was no significant association between HAGLR expression and histological grade and histological type. In addition, we detected the expression of HAGLR in gastric cancer cells. The results showed compared with normal gastric epithelial cell lines (GES-1), the expression levels of HAGLR were significantly increased in multiple GC cell lines, especially AGS and HGC-27 cells (Fig. 6O).

Silencing HAGLR significantly suppressed proliferation and migration in GC cells

To further explore the biological roles of HAGLR in GC progression, we established HAGLR knockdown cell lines. The transfection efficiency of HAGLR in AGS and HGC-27 cells was determined by RT−qPCR. The results indicated that HAGLR could be effectively knocked down by shHAGLR-1, shHAGLR-2, and shHAGLR-3 (Fig. 7A), and shHAGLR-2 and shHAGLR-3 were selected for functional experiments. The results of CCK8 assays showed that silencing HAGLR distinctly suppressed the viability of AGS and HGC-27 cells when compared with the control group (shCtrol) (Fig. 7B). Colony formation

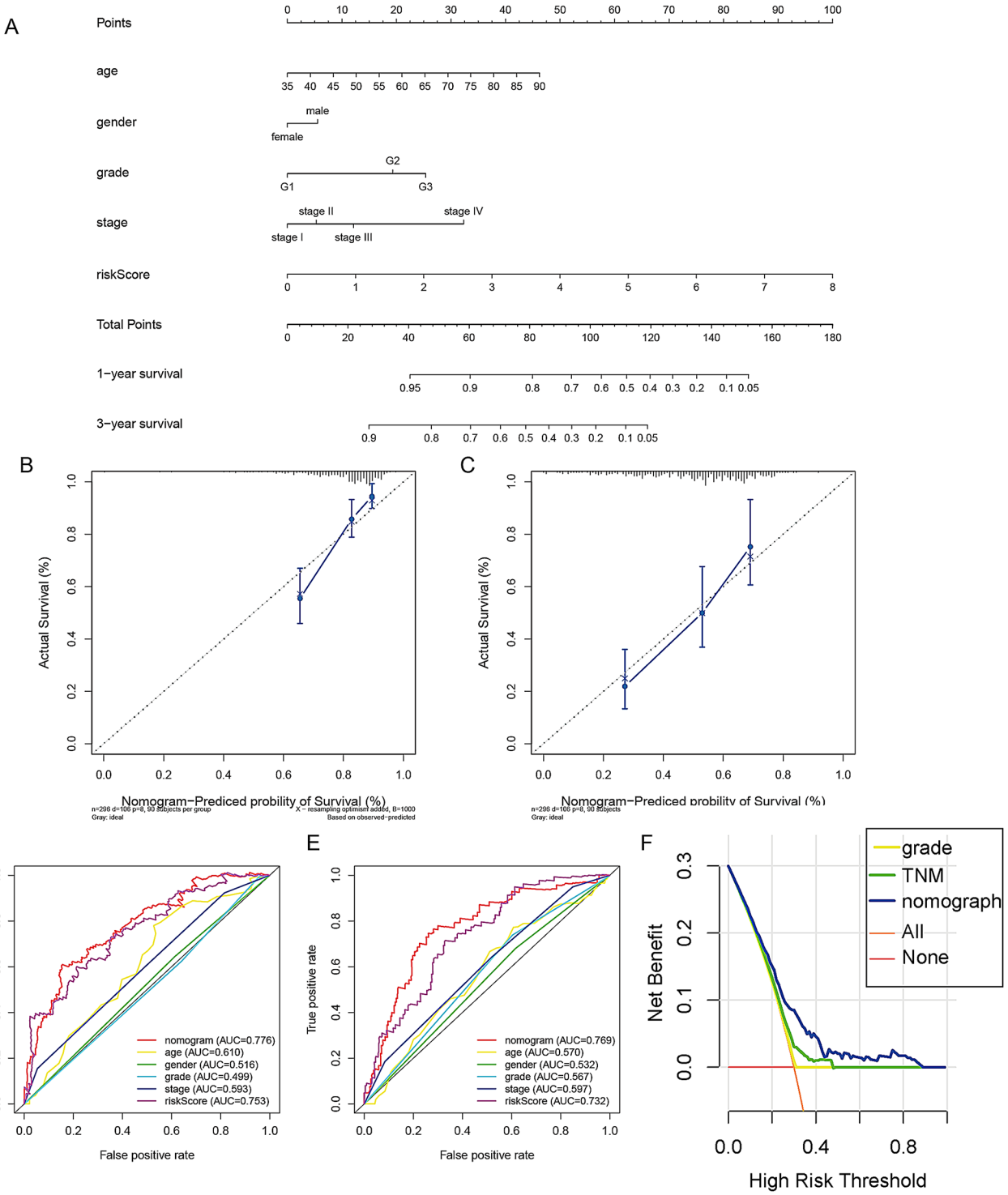

Fig. 5 Construction and verification of the predictive nomogram for patients with gastric cancer. **A**. Nomogram predicting the probability of 1- and 3-year OS for the prognosis of patients with gastric cancer; **B**-**C**. Calibration curve for the predictive accuracy of the nomogram. The Y-axis represents actual survival, and the X-axis represents nomogram-predicted survival; **D**-**E**.The receiver operating characteristic (ROC) curve analysis of the nomogram for 1- and 3-year OS; **F**. Decision curve analysis evaluating the clinical practicality of the nomogram model

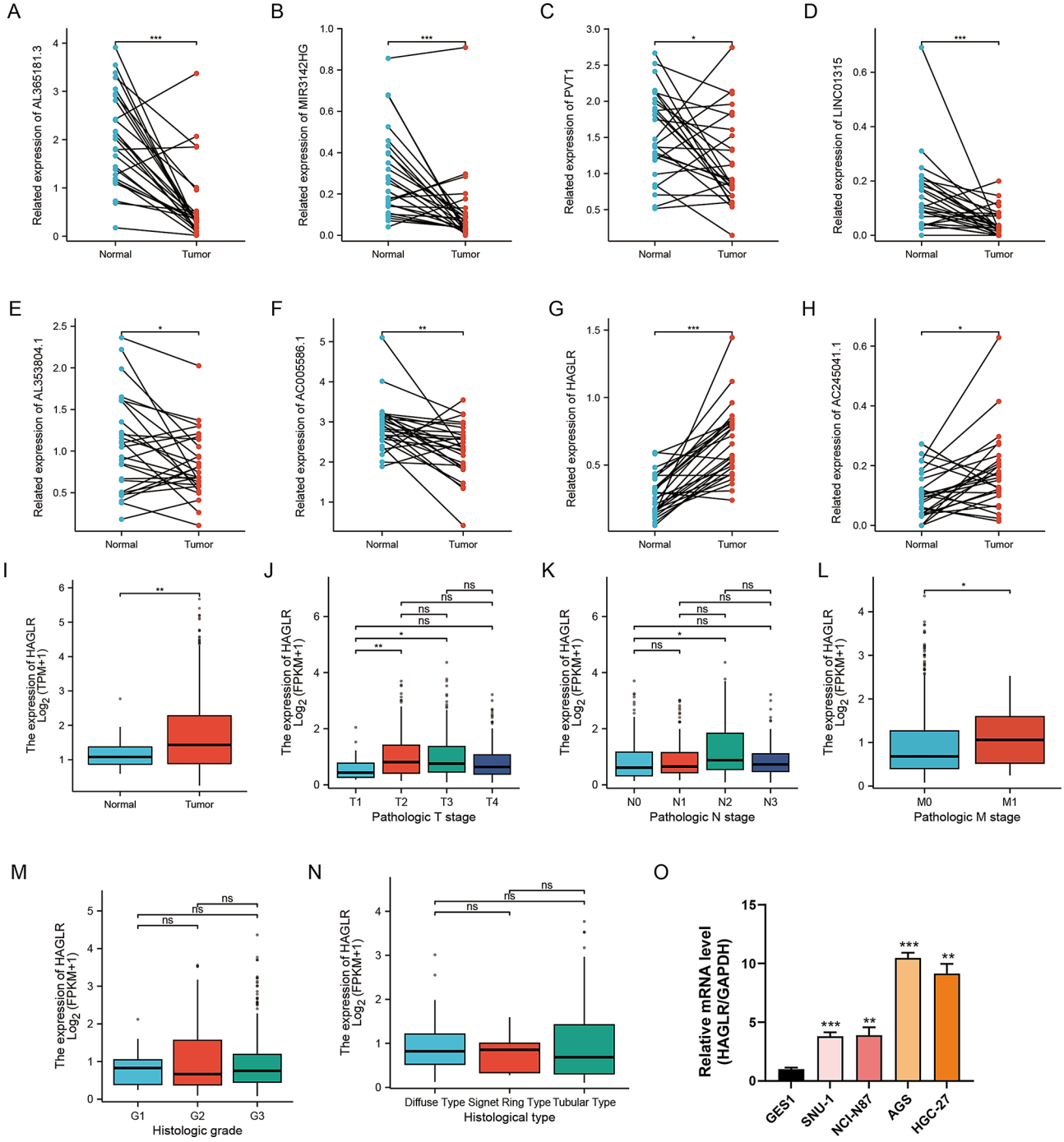

Fig. 6 The expression of ferroptosis-related lncRNAs in gastric cancer tissues and cells. **A**-**I**. The differential expression of the eight ferroptosis-related lncRNAs in 27 paired gastric cancer tissues and adjacent normal tissues ($n = 27$, $^{**}p < 0.01$,$^{***}p < 0.001$); **I**. The differential expression of HAGLR in 375 GC tissues and 32 normal tissues based on TCGA datasets ($^{**}p < 0.01$); **J**-**N**. The relationship between HAGLR expression levels and clinicopathologic features of GC patients based on TCGA datasets($^{*}p < 0.05$,$^{**}p < 0.01$); O. RT-qPCR analysis of HAGLR expression in gastric epithelial cell line GES-1, and four GC cell lines (SNU-1, NCI-N87, AGS, and HGC-27) (Mean ± SD, $n = 3$, $^{**}p < 0.01$,$^{***}p < 0.001$)

assays further indicated that loss of HAGLR significantly reduced the number of colonies formed by AGS and HGC-27 cells compared with cells transfected with control plasmids (Fig. 7C). Meanwhile, scratch wound-healing and transwell migration assays were conducted to discuss the effect of HAGLR on the migration of GC cells. The results of the wound-healing assay showed that migration capacity was weakened in AGS and HGC-27 cells transfected with shHAGLR-1 and shHAGLR-2 compared with that in the control group (Fig. 7D). Similarly,

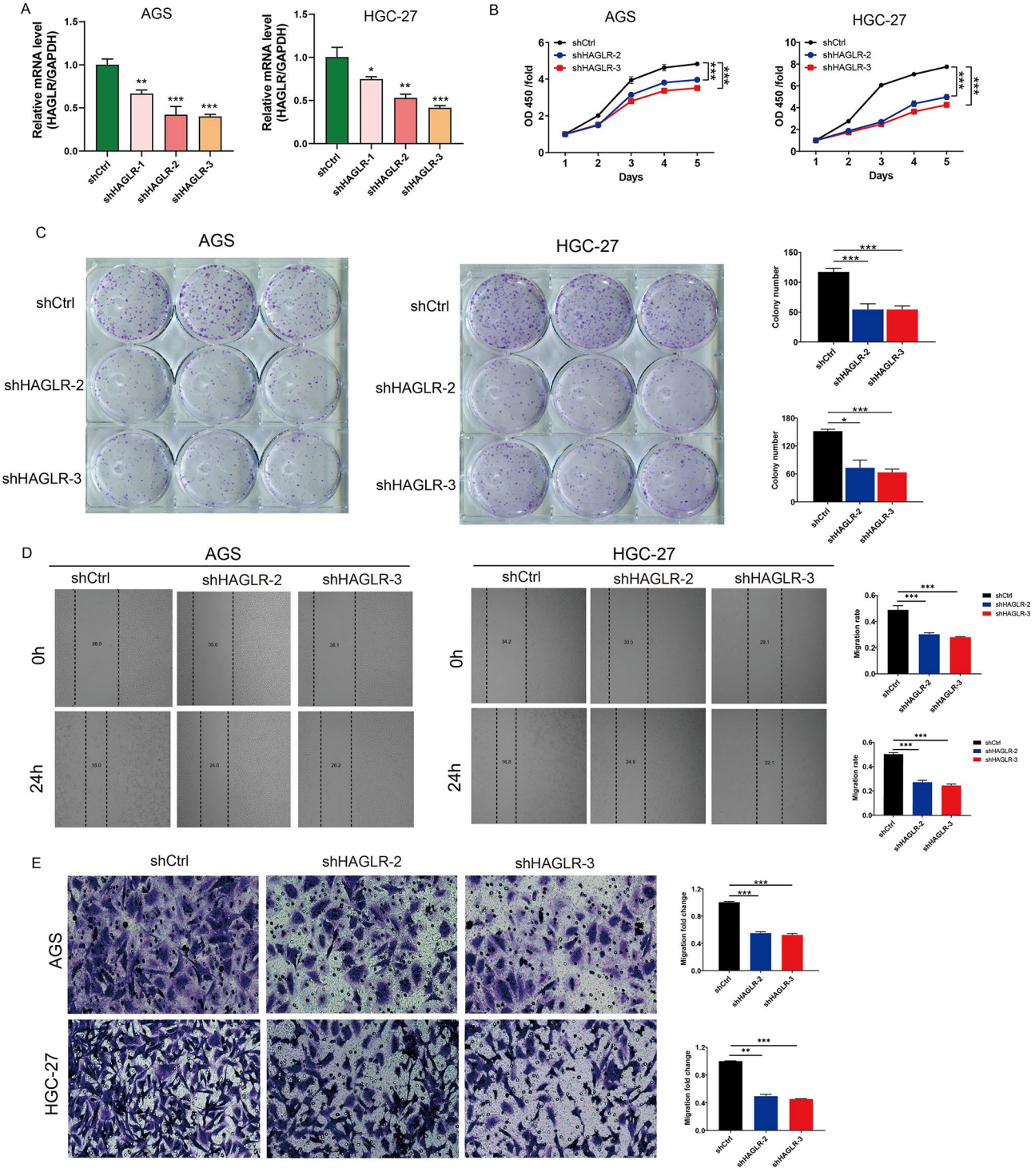

Fig. 7 Downregulation of HAGLR inhibits GC cells proliferation and migration. (**A**) The silence efficiency of different shHAGLR was evaluated by using RT-qPCR in AGS and HGC-27 cells(Mean ± SD, $n = 3$, $^{*}p < 0.05$,$^{**}p < 0.01$,$^{***}p < 0.001$); (**B**) Cell viability of AGS and HGC-27 cells transfected with shHAGLR or negative control (shCtrl) was detected by CCK8 (Mean ± SD, $n = 3$, $^{***}p < 0.001$); (**C**) Colony formation assays detected the cell growth ability of AGS and HGC-27 cells transfected with shHAGLR or negative control (shCtrl) (Mean ± SD, $n = 3$, $^{*}p < 0.05$, $^{***}p < 0.001$); (**D**) Migration ability was assessed by scratch wound-healing in AGS and HGC-27 cells transfected with shHAGLR or negative control (shCtrl), representative images (left) were shown (original magnification, ×100), and wound healing diameter were calculated (right) (Mean ± SD, $n = 3$, $^{***}p < 0.001$); E.Transwell assay was used to assess the migration ability of the AGS and HGC-27 cells transfected with shHAGLR or negative control (shCtrl); representative images(left) were shown (original magnification, ×200); the histograms (right) showed the number of migration cells(Mean ± SD, $n = 3$, $^{**}p < 0.001$, $^{***}p < 0.001$)

the transwell migration assay demonstrated that the number of migrated AGS and HGC-27 cells was dramatically reduced after HAGLR silencing (Fig. 7E). These results indicated that knockdown of HAGLR suppressed GC cell proliferation and migration.

Knockdown of HAGLR accelerated apoptosis and ferroptosis cell death process

To investigate the impact of HAGLR on apoptosis, we used the flow cytometry assay to examine apoptosis. The results revealed that the apoptosis ratio increased significantly after HAGLR silencing in AGS and HGC-27 cells, indicating that downregulation of HAGLH promoted GC cell apoptosis (Fig. 8A). Subsequently, to explore whether HAGLR affects the occurrence of ferroptosis, we detected ferroptosis-related markers, including intracellular ROS, GSH, free divalent iron, and lipid peroxide product MDA. The results showed treatment of AGS and HGC-27 cells with erastin (10μM) to induce ferroptosis exhibited the increased levels of ROS, MDA, and Fe2+, while decreased GSH level (Fig. 8B-E). Moreover, in the erastin-treated group, knocking down HAGLR in AGS and HGC-27 cells further increased the level of intracellular ROS (Fig. 8B), MDA (Fig. 8C), and Fe^{2+}(Fig. 8D), whereas decreased GSH content (Fig. 8E). Transmission electron microscopy results demonstrated that knocking down HAGLR induced the typical morphological changes of mitochondria, exhibiting smaller mitochondria, reduced mitochondria crista and ruptured outer membrane, indicative of ferroptosis occurrence (Fig. 8F-G). Moreover, we assessed the expression levels of key ferroptosis proteins (ACSL4 and GPX4), which play crucial roles in regulating ferroptosis. The results showed in the erastin-treated group, HAGLR knockdown in GC cells resulted in the upregulation of ACSL4 and downregulation of GPX4 (Fig. 8H-I).These results indicated that knockdown HAGLR promoted ferroptosis, suggesting that HAGLR may have an inhibitory effect on ferroptosis in GC cells.

Discussion

Gastric cancer (GC) is one of the most common malignancies worldwide with a high incidence and dismal prognosis. Most patients are diagnosed at advanced stages due to the lack of distinguishing clinical indicators [1]. Extensive studies suggest that ferroptosis plays a pivotal role in tumor suppression, thus providing new opportunities for cancer diagnosis and therapy [20]. Thus, we focused on ferroptosis as a breakthrough point to explore novel prognostic markers for GC. In our study, we constructed a prognostic risk model with eight ferroptosis-related lncRNAs for GC patients based on the TCGA database. We found that this prognostic model could accurately and independently predict OS in GC patients. Additionally, a key gene (HAGLR) of this risk model was selected for functional experimental verification.

Long noncoding RNAs(lncRNAs) have been shown to be involved in a variety of biological processes of GC progression, such as proliferation, invasion, chemotherapy resistance, as well as ferroptosis [21]. Lin Z et al. reported that under hypoxic conditions, lncRNA-PMAN regulates GC cells ferroptosis by increasing the stability of SLC7A11 and promotes peritoneal metastasis [22]. Huang et al. found that lncRNA BDNF-AS protected GC cells from ferroptosis and promoted the progression and peritoneal metastasis of GC [23]. Ferroptosis-related lncRNAs also serve as effective prognostic biomarkers and therapeutic targets for various tumors Nevertheless, the predictive value of ferroptosis-related lncRNAs in GC still needs to be further elucidated. Hence, in this study, we focused on the prognostic value of ferroptosis-related lncRNA signatures. In the primary cohort, we constructed a prognostic model with eight ferroptosis-related lncRNAs using Cox regression analysis. The Renyi weighted test showed that the survival of patients with GC in the high-risk group was worse than that in the low-risk group. Moreover, the prediction performance of this model was cross-validated by an internal data (validation set). We established a nomogram based on ferroptosis-related lncRNA risk signature and clinical features (age, sex, grade, clinical stage). All the verification results indicated that the nomogram showed better clinical practicality than the traditional predictions and satisfactory uniformity with actual survival. Generally, the risk model exhibited more sensitivity and specificity in predicting OS and acted as an independent prognostic factor for GC patients when compared with other clinical parameters. Nevertheless, we need more clinical samples to test the applicability of this risk signatures. In this study, we collected 27 gastric cancer tissue samples during surgical operations and detected expression level of the eight ferroptosis-related lncRNAs. Next, we will expand the sample size and follow-up time to further verify the accuracy of the risk model.

Some lncRNAs in this risk model have been validated as functional genomics in multiple tumors, including GC. It was reported that AL365181.3 is highly expressed in LUAD tissues, AL365181.3 knockdown reduced the proliferation, migration and invasion capacity of LUAD cells [24]. PVT1 promotes gemcitabine resistance of pancreatic cancer via up-regulating the expression of both Pygo2 and ATG14 and thus regulated Wnt/β-catenin signaling and autophagic activity [25]. PVT1 expression was significantly increased in osteosarcoma cells, knocking down PVT1 markedly inhibited the cell proliferation, migration, and invasion, while promoted ferroptosis through activating STAT3/GPX4 axis [26]. LINC01315 was found

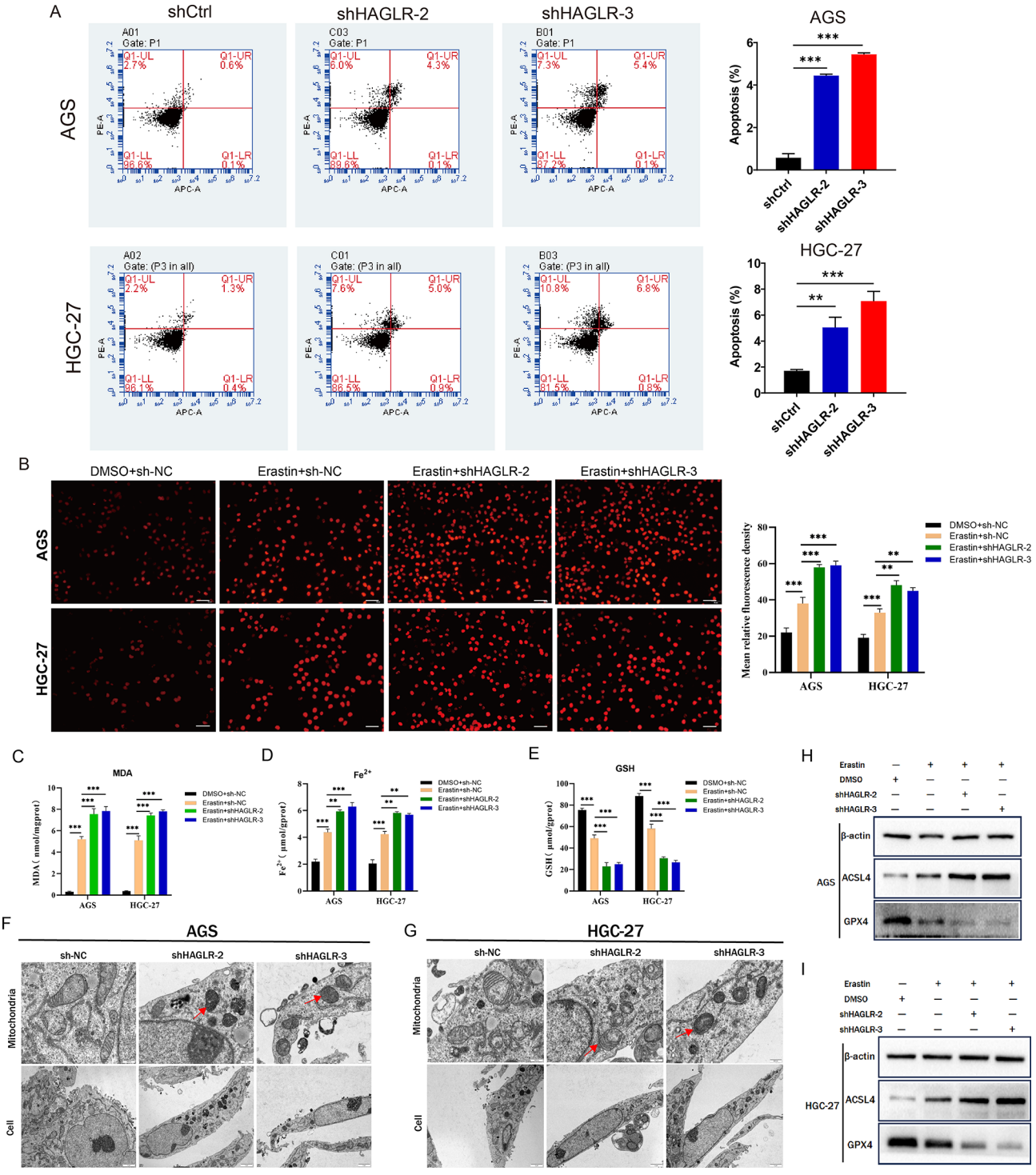

Fig. 8 Silencing HAGLR inhibits GC cells migration. Silencing HAGLR promoted GC cells apoptosis and ferroptosis. **A**. Flow cytometry assay evaluate the apoptosis rate in AGS and HGC-27 cells treated with shHAGLR or negative control (shCtrl) (Mean ± SD, $n = 3$, $^{**}p < 0.01$, $^{***}p < 0.001$); **B**-E. The effects of HAGLR knockdown on intracellular ROS(B), MDA(C), Fe^{2+}(D), GSH(E) (The scale bar: 50 μm, Mean ± SD, $n = 3$, $^{**}p < 0.01$, $^{***}p < 0.001$); **F**-**G**. The effects of HAGLR knockdown on mitochondrial morphology (The scale bar in cell is 2μ, in Mitochondria is 50° nm); **H**-**I**. The effects of HAGLR knockdown on ferroptosis related proteins ACSL4 and GPX4

to be poorly expressed in oral squamous cell carcinoma (OSCC), and LINC01315 knockdown enhanced OSCC cell proliferation, invasion, and migration but dampened apoptosis via the miR-211/DLG3 axis [27]. Conversely, in colorectal carcinoma (CRC), LINC01315 was significantly upregulated and facilitated the growth and invasive phenotypes of CRC cells by sponging miR-205-3p. HAGLR has been reported to be upregulated in various malignant tumors and to promote tumor progression, such as esophageal cancer [28], hepatocellular carcinoma [29], colon cancer [30], thyroid cancer [31], and breast cancer [32]. In GC, HAGLR promotes 5-Fu resistance by sponging miR-338-3p and targeting the LDHA-glycolysis pathway [33]. In this study, we discovered that the expression of AL365181.3, MIR3142HG, PVT1, LINC01315, AL353804.1, and AC005586.1 was downregulated in GC tissues and showed a positive correlation with survival time, whereas HAGLR and AC245041.1 was highly expressed in GC tissues and associated with poor survival. In addition, we focused specifically on the biological role of HAGLR in GC. We discovered that HAGLR was highly expressed in multiple GC cells, silencing HAGLR could effectively inhibit the proliferation and migration, and promote the apoptosis and ferroptosis of GC cells, suggesting that HAGLR may be a promising target for GC treatment.

Ferroptosis is a newly regulated cell death mechanism driven by oxidative injury and promotes polyunsaturated fatty acids (PUFAs) peroxidation in an iron-dependent accumulation, tightly linked with metabolic pathways. The ferroptosis process is regulated by multiple positive and negative factors, which involves ferrous iron accumulation, free radical production, antioxidant system dysfunction, and lipid peroxidation [34]. Numerous studies supports the notion that ferroptosis acts as a natural antitumor mechanism [35]. Intriguingly, specific oncogenes mutations tend to endow cancer cells with the ability to evade ferroptosis. A prominent example linking ferroptosis to tumor suppression is p53, which plays a pivotal role in inhibting tumor growth. A p53 mutant proteins, $p53^{R273H}$, acts as a repressor for ferroptosis by abrogating BACH1-mediated downregulation of SLC7A11 to enhance tumor growth [36]. In the acetylationdefective p53 mouse models, p53-mediated ferroptosis is implicated as critical component of in tumor suppression [35]. Several metabolic targets of p53, such as VKORC1L1, PLTP, SLC7A11, and GLS2, are also directly involved in modulating ferroptosis [35]. In our analysis, we found p53 signaling pathway is enriched in the low-risk group, which may account for why patients in low-risk group have a better overall survival. Whereas, the related mRNAs in the high-risk group was mainly involved in the Hippo signaling pathway, which aslo plays a critical role in modulating ferroptosis susceptility. In low cell density condition, the Hippo pathway is inactivated, the major downstream effector TAZ accumulates in the nucleus, which leading to TAZ transcriptionally activate EMP1 and induced ferroptosis in renal cell carcinoma [37]. In epithelial cells, E-cadherin suppress ferroptosis by activating the intracellular NF2 and Hippo signalling pathway, while blocking the NF2-Hippo axis allows the YAP promoting ferroptosis via up-regulation of ferroptosis regulator ACSL4 and TFRC [38]. Overall, the patients in high-risk group may be prone to developing ferroptosis resistance. Moreover, in the experimental validation, we discovered knockdown of HAGLR, which is the key gene responsible for the increased risk score, increased the level of ferroptosis-related markers, including ROS, MDA, and Fe2+, whereas decreased GSH level.

The relationship between ferroptosis and tumor immunity has aroused extensive interest in recent years. On the one hand, the susceptibility to ferroptosis varies significantly across immune cells, and different types of immune cells can either enhance or inhibit ferroptosis in cancer cells. On the other hand, ferroptosis in cancer cells might influence immune responses [35]. Recent investigations have reported that M1 tumor-associated macrophages(TAMs) display greater resistance to ferroptosis than do M2 TAMs. As a results, ferroptosis inducing therapies may selectively reduce M2 TAMs without impacting M1 TAMs [39]. The ssGSEA results in our study showed macrophages was enriched in high-risk group with less ferroptosis, that may indicated the proportion of immunosuppressive M2 macrophages is increased in high-risk patients, and resulting in an poor survival. Besides, dysfunctional NK cell were found to be associated with lipid peroxidation-driven oxidative stress; ferroptosis inhibition increases NK cell survival in tumors [35]. In this study, we found the high-risk group with ferroptosis inhibition exhibited marked enrichment of NK cells. Likewise, various cytokines secreted by different immune cells are able to promote or suppress ferroptosis. IFN-γ released from activated CD8 + T cells inhibits cystine uptake by downregulating SLC7A11 expression and augmenting ACSL4 expression, thereby facilitating lipid peroxidation and induces ferroptosis in cancer cells [40]. Together, the ferroptosis and immune status is associated with the prognosis of GC patients. While the complex connection between tumor immunity and ferroptosis needs to be further studied.

Although we established a prognostic signature and the nomogram performed well in predicting the survival of patients with GC, the limitations of our study deserve attention. First, this eight ferroptosis-related lncRNA prognostic signature was constructed and evaluated using limited data and clinical information from the TCGA database and was not verified in external cohorts, which restricted the practicality and generalizability of

the prognostic model. Moreover, some of these lncRNAs have rarely been reported and are worthy of further research. It is critical to verify these bioinformatics prediction results with functional experiments and molecular mechanism studies of the eight ferroptosis-related lncRNAs.

Conclusion

We constructed and identified a novel ferroptosis-related prognostic risk model comprising eight lncRNAs (AL365181.3, MIR3142HG, PVT1, LINC01315, AL353804.1, HAGLR, AC005586.1, and AC245041.1) in GC. Additionally, our study demonstrated that HAGLR plays an important role in GC progression and regulating ferroptosis, which may become a promising therapeutic target for GC patients.

Abbreviations

GC	Gastric cancer
LncRNA	Long non-coding RNA
TCGA	The Cancer Genome Atlas
HR	Hazard ratio
OS	Overall survival
ROC	Receiver operating characteristic
multi-ROC	Multi-indicator receiver operating characteristic
AUC	Area under the curve
DCA	Decision curve analysis
GSEA	Gene set enrichment analysis
ssGSEA	Single-sample gene set enrichment analysis
CI	Confidence Interval
HR	Hazard Ratio

Supplementary Information

The online version contains supplementary material available at https://doi.org/10.1186/s12876-025-03951-7.

Supplementary figure S1. Construction of ferroptosis-related LncRNAs with independent prognosis in gastric cancer. The forest plot showed the Hazard Ratio (95% Confidence Interval) and ***p*** value of lncRNAs by multivariate Cox proportional hazards analysis.

Supplementary figure S2 Co-expression network of the prognostic ferroptosis-related lncRNAs-mRNAs visualized using Cytoscape(A) and Sankey diagram(B)

Supplementary figure S3. Stratification analysis of the correlation between the risk groups and survival based on age, gender, grade, and clinical stage A. Age ≤ 65; B: Age > 65; C: Male; D: Female; E: Grade 1–2; F: Grade 3; G: Stage I-II; H: Stage III-IV.

Supplementary figure S4. Enrichment analysis and immune state analysis of the prognostic ferroptosis-related signature in gastric cancer. A-B. Comparison the biological pathways and function between low- and high-risk groups according to GSEA analysis(A) and Gene Ontology (GO) analysis(B); C. Comparison of the infiltration levels of 16 immune cells between low- and high-risk groups. D. Comparison of the immune functions between low- and high-risk groups. ns: no significance; *$p < 0.05$; **$p < 0.01$; ***$p < 0.001$.

Supplementary Material 5

Supplementary Material 6

Supplementary Material 7

Acknowledgements

Not applicable.

Author contributions

Shenglan Huang: Conceptualization, Methodology, Data curation, Validation, Funding acquisition, Writing–original draft. K L: Methodology, Data curation, Validation, Visualization, Investigation. Queling Liu: Data curation, Investigation. Si Tao: Investigation, Format analysis. Hua Wang: Supervision, Project administration. All authors read and approved the final manuscript.

Funding

Disclosure.
This research was supported by the Science and Technology Project of Jiangxi Provincial Department of Education (No. GJJ2400117), and the National Natural Science Foundation incubation project of The Second Affiliated Hospital of Nanchang University (No. 2023YNFY12031).

Data availability

The datasets presented in this study can be found in online repositories. The names of the repository/repositories and the project name can be found in The Cancer Genome Atlas database (https://portal.gdc.cancer.gov/). The raw data are available from the corresponding author on reasonable request.

Declarations

Ethical approval

This study involving human participants was reviewed and approved by the Second Affiliated Hospital of Nanchang University Medical Research Ethics Committee. The patients/participants provided written informed consent to participate in this study.

Consent for publication

Not applicable.

Competing interests

The authors declare no competing interests.

Received: 21 June 2024 / Accepted: 29 April 2025
Published online: 08 May 2025

References

1. Guan WL, He Y, Xu RH. Gastric cancer treatment: recent progress and future perspectives. J Hematol Oncol. 2023;16(1):57.
2. Duraes C, Almeida GM, Seruca R, Oliveira C, Carneiro F. Biomarkers for gastric cancer: prognostic, predictive or targets of therapy? Virchows Arch. 2014;464(3):367–78.
3. Tirada N, Aujero M, Khorjekar G, Richards S, Chopra J, Dromi S, et al. Breast Cancer tissue markers, genomic profiling, and other prognostic factors: A primer for radiologists. Radiographics. 2018;38(7):1902–20.
4. Dixon SJ, Lemberg KM, Lamprecht MR, Skouta R, Zaitsev EM, Gleason CE, et al. Ferroptosis: an iron-dependent form of nonapoptotic cell death. Cell. 2012;149(5):1060–72.
5. Yang WS, Kim KJ, Gaschler MM, Patel M, Shchepinov MS, Stockwell BR. Peroxidation of polyunsaturated fatty acids by lipoxygenases drives ferroptosis. Proc Natl Acad Sci U S A. 2016;113(34):E4966–75.
6. Shi Z, Zhang L, Zheng J, Sun H, Shao C. Ferroptosis: biochemistry and biology in cancers. Front Oncol. 2021;11:579286.
7. Li D, Wang Y, Dong C, Chen T, Dong A, Ren J, et al. CST1 inhibits ferroptosis and promotes gastric cancer metastasis by regulating GPX4 protein stability via OTUB1. Oncogene. 2023;42(2):83–98.
8. Gu R, Xia Y, Li P, Zou D, Lu K, Ren L, et al. Ferroptosis and its role in gastric Cancer. Front Cell Dev Biol. 2022;10:860344.
9. Jiang X, Yan Q, Xie L, Xu S, Jiang K, Huang J, et al. Construction and validation of a Ferroptosis-Related prognostic model for gastric Cancer. J Oncol. 2021;2021:6635526.
10. Huo J, Wu L, Zang Y. Eight-gene prognostic signature associated with hypoxia and ferroptosis for gastric cancer with general applicability. Epigenomics. 2021;13(11):875–90.

11. Song S, Shu P. Expression of ferroptosis-related gene correlates with immune microenvironment and predicts prognosis in gastric cancer. Sci Rep. 2022;12(1):8785.
12. Zheng JJ, Wang JP. Identification of ferroptosis-related genes for the prediction of prognosis and chemotherapy benefit of gastric cancer. Eur Rev Med Pharmacol Sci. 2022;26(18):6754–63.
13. Deng X, Bi Q, Chen S, Chen X, Li S, Zhong Z, et al. Identification of a Five-Autophagy-Related-lncRNA signature as a novel prognostic biomarker for hepatocellular carcinoma. Front Mol Biosci. 2020;7:611626.
14. Yuan L, Xu ZY, Ruan SM, Mo S, Qin JJ, Cheng XD. Long non-coding RNAs towards precision medicine in gastric cancer: early diagnosis, treatment, and drug resistance. Mol Cancer. 2020;19(1):96.
15. Park EG, Pyo SJ, Cui Y, Yoon SH, Nam JW. Tumor immune microenvironment LncRNAs. Brief Bioinform. 2022;23(1).
16. Xu Z, Peng B, Liang Q, Chen X, Cai Y, Zeng S, et al. Construction of a Ferroptosis-Related Nine-lncRNA signature for predicting prognosis and immune response in hepatocellular carcinoma. Front Immunol. 2021;12:719175.
17. Wu Z, Lu Z, Li L, Ma M, Long F, Wu R, et al. Identification and validation of Ferroptosis-Related LncRNA signatures as a novel prognostic model for Colon cancer. Front Immunol. 2021;12:783362.
18. Tang Y, Li C, Zhang YJ, Wu ZH. Ferroptosis-Related long Non-Coding RNA signature predicts the prognosis of head and neck squamous cell carcinoma. Int J Biol Sci. 2021;17(3):702–11.
19. Zhou N, Bao J. FerrDb: a manually curated resource for regulators and markers of ferroptosis and ferroptosis-disease associations. Database: the journal of biological databases and curation. 2020;2020.
20. Zhang C, Liu X, Jin S, Chen Y, Guo R. Ferroptosis in cancer therapy: a novel approach to reversing drug resistance. Mol Cancer. 2022;21(1):47.
21. Hosseini SA, Haddadi MH, Fathizadeh H, Nemati F, Aznaveh HM, Taraj F, et al. Long non-coding RNAs and gastric cancer: an update of potential biomarkers and therapeutic applications. Volume 163. Biomedicine & pharmacotherapy = Biomedecine & pharmacotherapie; 2023. p. 114407.
22. Lin Z, Song J, Gao Y, Huang S, Dou R, Zhong P, et al. Hypoxia-induced HIF-1α/lncRNA-PMAN inhibits ferroptosis by promoting the cytoplasmic translocation of ELAVL1 in peritoneal dissemination from gastric cancer. Redox Biol. 2022;52:102312.
23. Huang G, Xiang Z, Wu H, He Q, Dou R, Lin Z, et al. The LncRNA BDNF-AS/WDR5/FBXW7 axis mediates ferroptosis in gastric cancer peritoneal metastasis by regulating VDAC3 ubiquitination. Int J Biol Sci. 2022;18(4):1415–33.
24. Liu X, Liu J, Zeng Y, Qiao D, Wang Q. AL365181.3 as a novel prognostic biomarker for lung adenocarcinoma. Sci Rep. 2025;15(1):5853.
25. Zhou C, Yi C, Yi Y, Qin W, Yan Y, Dong X, et al. LncRNA PVT1 promotes gemcitabine resistance of pancreatic cancer via activating Wnt/β-catenin and autophagy pathway through modulating the miR-619-5p/Pygo2 and miR-619-5p/ATG14 axes. Mol Cancer. 2020;19(1):118.
26. Li G, Feng J, Huang S, Li Q. LncRNA-PVT1 inhibits ferroptosis through activating STAT3/GPX4 Axis to promote osteosarcoma progression. Front Bioscience (Landmark edition). 2024;29(6):207.
27. Chen FB, Wu P, Zhou R, Yang QX, Zhang X, Wang RR, et al. LINC01315 impairs microRNA-211-Dependent DLG3 downregulation to inhibit the development of oral squamous cell carcinoma. Front Oncol. 2020;10:556084.
28. Yang C, Shen S, Zheng X, Ye K, Sun Y, Lu Y, et al. Long noncoding RNA HAGLR acts as a microRNA-143-5p sponge to regulate epithelial-mesenchymal transition and metastatic potential in esophageal cancer by regulating LAMP3. Faseb J. 2019;33(9):10490–504.
29. Li YH, Huang GM, Wang W, Zang HL. LncRNA HAGLR exacerbates hepatocellular carcinoma through negatively regulating miR-6785-5p. Eur Rev Med Pharmacol Sci. 2020;24(18):9353–60.
30. Sun W, Nie W, Wang Z, Zhang H, Li Y, Fang X. Lnc HAGLR promotes Colon cancer progression through sponging miR-185-5p and activating CDK4 and CDK6 in vitro and in vivo. Onco Targets Ther. 2020;13:5913–25.
31. Dong L, Geng Z, Liu Z, Tao M, Pan M, Lu X. IGF2BP2 knockdown suppresses thyroid cancer progression by reducing the expression of long non-coding RNA HAGLR. Pathol Res Pract. 2021;225:153550.
32. Jin L, Luo C, Wu X, Li M, Wu S, Feng Y. LncRNA-HAGLR motivates triple negative breast cancer progression by regulation of WNT2 via sponging miR-335-3p. Aging. 2021;13(15):19306–16.
33. Hu J, Huang L, Ding Q, Lv J, Chen Z. Long noncoding RNA HAGLR sponges miR-338-3p to promote 5-Fu resistance in gastric cancer through targeting the LDHA-glycolysis pathway. Cell Biol Int. 2022;46(2):173–84.
34. Zhou Q, Meng Y, Li D, Yao L, Le J, Liu Y, et al. Ferroptosis in cancer: from molecular mechanisms to therapeutic strategies. Signal Transduct Target Therapy. 2024;9(1):55.
35. Lei G, Zhuang L, Gan B. The roles of ferroptosis in cancer: tumor suppression, tumor microenvironment, and therapeutic interventions. Cancer Cell. 2024;42(4):513–34.
36. Su Z, Kon N, Yi J, Zhao H, Zhang W, Tang Q, et al. Specific regulation of BACH1 by the hotspot mutant p53(R175H) reveals a distinct gain-of-function mechanism. Nat cancer. 2023;4(4):564–81.
37. Magesh S, Cai D. Roles of YAP/TAZ in ferroptosis. Trends Cell Biol. 2022;32(9):729–32.
38. Wu J, Minikes AM, Gao M, Bian H, Li Y, Stockwell BR, et al. Intercellular interaction dictates cancer cell ferroptosis via NF2-YAP signalling. Nature. 2019;572(7769):402–6.
39. Zhao L, Zhou X, Xie F, Zhang L, Yan H, Huang J, et al. Ferroptosis in cancer and cancer immunotherapy. Cancer Commun (London England). 2022;42(2):88–116.
40. Liao P, Wang W, Wang W, Kryczek I, Li X, Bian Y, et al. CD8(+) T cells and fatty acids orchestrate tumor ferroptosis and immunity via ACSL4. Cancer Cell. 2022;40(4):365–e786.

Publisher's note